

Chaperonin GroEL GroES Functions as both Alternating and Non-Alternating Engines

著者	Yamamoto Daisuke, Ando Toshio
journal or publication title	Journal of Molecular Biology
volume	428
number	15
page range	3090-3101
year	2016-07-31
URL	http://hdl.handle.net/2297/46170

doi: 10.1016/j.jmb.2016.06.017

1 Chaperonin GroEL–GroES Functions as both Alternating and Non-Alternating
2 Engines

3

4 Daisuke Yamamoto^{1,2,3} and Toshio Ando^{1,2}

5

6 ¹Department of Physics, Kanazawa University, Kakuma-machi, Kanazawa 920-1192, Japan

7 ²CREST, JST, Sanban-cho, Chiyoda-ku, Tokyo 102-0075, Japan

8 ³Present address: Department of Applied Physics, Fukuoka University, Nakakuma, Jyonan-ku,
9 Fukuoka 814-0180, Japan

10 Correspondence to Toshio Ando: tando@staff.kanazawa-u.ac.jp

11

12

13 **Abstract**

14

15 A double ring-shaped GroEL consisting of 14 ATPase subunits assists protein folding,
16 together with co-chaperonin GroES. The dynamic GroEL–GroES interaction is actively
17 involved in the chaperonin reaction. Therefore, revealing this dynamic interaction is a key to
18 understanding the operation principle of GroEL. Nevertheless, how this interaction proceeds
19 in the reaction cycle has long been controversial. Here, we directly imaged GroEL–GroES
20 interaction in the presence of disulfide-reduced α -lactalbumin as a substrate protein, using
21 high-speed atomic force microscopy. This real-time imaging revealed occurrence of the
22 primary symmetric GroEL:GroES₂ and second-primary asymmetric GroEL:GroES₁
23 complexes. Remarkably, the reaction was observed to often branch into main and side
24 pathways. In the main pathway alternate binding and release of GroES occurs at the two rings,
25 indicating tight cooperation between the two rings. In the side pathway, however, this
26 cooperation is disrupted, resulting in interruption of the alternating rhythm. From various
27 properties observed for both pathways, we provide mechanistic insight into the alternate and
28 non-alternate operations of the two-engine system.

29

30

31

32 **Abbreviations used:** HS-AFM, high-speed atomic force microscopy; 2D, two-dimensional

33

34 **Introduction**

35

36 Chaperonins are a structurally conserved class of molecular chaperones that mediate
37 protein folding to the native functional state in cells [1,2]. The best studied chaperonin,
38 *Escherichia coli*. GroEL, is a cylindrical protein complex formed by two heptameric rings
39 stacked back to back, each consisting of identical ATPase subunits [3]. GroEL functions
40 together with the lid-like co-chaperonin GroES. GroES is a single homo-heptameric ring and
41 binds to the ends of the GroEL cylinder depending on the nucleotide state of GroEL. The
42 mechanism of productive protein folding assisted by GroEL and GroES has been studied
43 extensively [4–6]. Nonnative, unfolded proteins with exposed hydrophobic residues bind to
44 GroEL at its apical domain that presents a hydrophobic surface for this binding [7]. Then, the
45 substrate protein is encapsulated into the hydrophilic cavity of GroEL upon its binding to ATP
46 and GroES, accompanied by a large conformational change of GroEL [8,9]. The encapsulated
47 protein can fold in this environment taking several seconds, the time needed for one ATP
48 turnover cycle to be completed in the GroES-bound ring. Subsequently, GroES dissociates
49 and then the substrate protein is released from GroEL. Because the two rings of GroEL are
50 identical, these processes proceed at each ring of GroEL.

51 However, how the reaction cycle proceeds in the “two-engine” system has long been
52 controversial. In a widely accepted model, it is postulated that only one ring binds GroES
53 throughout the cycle, so that asymmetric GroEL:GroES₁ complexes (referred to as the bullet
54 complexes) are exclusively formed in the steady-state ATPase cycle. The origin of this
55 asymmetry has been considered to be negative cooperativity between the rings regarding ATP
56 binding [10–12]. That is, only one ring can bind ATP, resulting in exclusive formation of the
57 bullet complexes because GroES can only bind to the ATP-bound ring [13], although GroES
58 is thought to be able to bind to the ADP–Pi-bound ring as well. Only after the bound ATP is
59 hydrolyzed in the GroES-bound ring (*cis*-ring), the opposite GroES-free ring (*trans*-ring) can
60 bind ATP. Actual ATP binding to the *trans*-ring induces release of GroES, ADP and the
61 encapsulated substrate protein from the opposite ring [14,15], while the second GroES binds
62 to the *trans*-ring to form a new *cis*-ring. Thus, this model has concluded that the two rings of
63 GroEL alternately bind and release GroES and hence alternately function. In another model,
64 however, both rings of GroEL are supposed to be able to bind ATP simultaneously and hence
65 also GroES to form symmetric GroEL:GroES₂ complexes (referred to as the football
66 complexes). Several lines of evidence have been provided for the existence of a large

67 population of the football complexes in the presence of ATP [16–27]. However, this model
68 has not gained broad consensus. This is mainly because the methods used hardly allow
69 directly detecting dynamic molecular events occurring at each ring.

70 Here, using high-speed atomic force microscopy (HS-AFM) [28,29] we directly observed
71 dynamic GroES association and dissociation events at each ring of individual GroEL
72 molecules during the steady-state ATPase cycle in the presence of disulfide-reduced
73 α -lactalbumin. HS-AFM is now established and has recently been used with great success to
74 visualize protein molecules in dynamic action [30–32]. The GroEL–GroES interaction was
75 previously observed by HS-AFM during the course of establishment of this microscopy
76 [33,34]. However, in these studies GroEL was immobilized in an end-up orientation on a mica
77 surface, making it infeasible to study the two-engine cycle. In the present study, we used
78 streptavidin two-dimensional (2D) crystals as a substrate, onto which GroEL molecules were
79 immobilized in a side-on orientation through the streptavidin-biotin linkage [35]. This system
80 allowed us to study the dynamic GroEL–GroES interaction occurring during the two-engine
81 cycle at a nearly saturating concentration of GroES. The HS-AFM imaging of the
82 GroEL–GroES interaction in the steady-state ATPase cycle revealed various properties of the
83 interaction, and thus, provided mechanistic insight into the two-engine cycle, as follows. The
84 symmetric football complex is primarily formed, while the two engines operate alternately in
85 a main pathway but non-alternately and non-simultaneously in a side pathway. The alternate
86 operation in the main pathway is made possible by inter-ring communications; ATP hydrolysis
87 into ADP–Pi in one ring triggers GroES dissociation from the opposite ring, while the
88 resulting asymmetric bullet structure retards ADP dissociation from the *trans*-ring. This
89 retardation can contribute to providing an enough time for the substrate protein to be released
90 from the *trans*-ring but in turn could possibly result in frequent, incomplete nucleotide
91 replacement of ADP with ATP at the *trans*-ring. By this incomplete exchange, the inter-ring
92 communication is very likely to be vanished, and therefore, the reaction pathway is
93 side-tracked into the side pathway.

94

95 **Results**

96

97 **Patterns of dynamic GroEL–GroES interaction**

98 For HS-AFM visualization of dynamic GroEL–GroES interaction at the two rings of
99 GroEL, the D490C GroEL mutant biotinylated at Cys490 was immobilized in a side-on

100 orientation on the streptavidin 2D crystal surface [35,36] (Fig. 1A). Since this surface is
101 highly resistant to nonspecific protein binding [35], GroES appeared in HS-AFM images only
102 when it was bound to the immobilized GroEL. This property allowed for the use of a high
103 concentration of GroES (1 μM), unlike conventional single-molecule fluorescence
104 microscopy. Figure 1B presents HS-AFM images that were captured at ~ 4 frames/s (fps) for
105 dynamic GroEL–GroES interaction in the presence of ATP and a substrate protein,
106 disulfide-reduced α -lactalbumin (Movie S1). The successive images clearly displayed
107 multiple rounds of GroES association/dissociation events at each ring of GroEL (Fig. 1B,C).

108 In the repeated cycles, the symmetric football complexes appeared most frequently
109 ($\sim 67\%$), while the bullet complexes appeared moderately ($\sim 33\%$) (Fig. 2A), consistent with a
110 previous electron microscopy study [37]. Next, we analyzed the order of association and
111 dissociation of GroES at the two rings by choosing the bullet complexes as an initial state (Fig.
112 2B). These dynamic events observed are largely classified into Type I and Type II; in Type I
113 the *cis/trans* states interchange between the two rings after a round of association and
114 dissociation of GroES, resulting in the polarity change between the initial and second bullet
115 complexes, whereas in Type II no *cis/trans* interchange occurs, resulting in no change of the
116 polarity. The probabilities of occurrence of Type I and Type II processes are ~ 0.69 and ~ 0.31 ,
117 respectively. These processes mostly proceeded through formation of the football complexes
118 (Fig. 2Bb,Be). In a less extent, no intermediate state appeared in Type I process (Fig. 2Bc). In
119 addition, processes going through the GroES-free state were only rarely observed (Fig.
120 2Ba,Bd). As described later, the occurrence of the two types of processes, Type I and Type II,
121 is not an artifact that might arise from missing capturing the second bullet complexes possibly
122 due to insufficient temporal resolution but consistent with a previous single-molecule
123 fluorescent microscopy study [21].

124

125 **Decay kinetics of football and bullet complexes**

126 The football complexes formed in Type I and Type II processes are apparently the same
127 but different species, as revealed by their distinct decay kinetics. The histogram of lifetime for
128 the football complex in Type I process (hereafter we refer to as Type I football) was well fitted
129 to a single-exponential function with a rate constant of $k^{\text{F-I}} = 0.49 \text{ s}^{-1}$ ($\chi^2 = 0.84$, $p > 0.71$)
130 (Fig. 3A, blue line), so that Type-I football decays in the first-order reaction. By contrast, the
131 histogram of lifetime for the football complex in Type II process (we refer to as Type-II
132 football) showed a maximum at ~ 2 s and was well fitted to a curve obtained for a sequential

133 two-step reaction with rate constants of $k^{F-II}_1 = 1.14 \text{ s}^{-1}$ and $k^{F-II}_2 = 0.59 \text{ s}^{-1}$ ($\tilde{\chi}^2 = 1.46$, $p =$
134 0.054) (Fig. 3B, blue lines; Note S1). This suggests that in Type II process the dissociation of
135 the second bound GroES is likely to be caused by certain reactions occurring in its bound ring
136 with the rate constants, k^{F-II}_1 and k^{F-II}_2 , as the decay process of Type II football is identical to a
137 process that leads to dissociation of the second bound GroES, unlike in Type I process where
138 the decay of Type I football occurs by dissociation of the early bound GroES.

139 Supposing that Type II football is apparently formed due to missing capturing the bullet
140 complex that occurs on route to the formation of the second football complex, its lifetime
141 should be approximately $2/k^{F-I} = 4.08 \text{ s}$ and its decay kinetics should follow a sequential
142 two-step reaction with the same rate constant identical to $k^{F-I} = 0.49 \text{ s}^{-1}$. Because the decay
143 kinetics exhibited by Type II football is largely inconsistent with these features, Type II
144 football is a real entity.

145 Next, we analyzed the decay kinetics of the bullet complexes to obtain a clue to an origin
146 of the formation of the two types of football complexes. The lifetime of the bullet complex
147 that was followed by Type I football was well fitted to a single-exponential function with a
148 rate constant of $k^{B-I} = 2.75 \text{ s}^{-1}$ ($\tilde{\chi}^2 = 0.48$, $p > 0.94$) (Fig. 3C, blue line). Also the lifetime of
149 the bullet complex that was followed by Type II football was well fitted to a
150 single-exponential function but its rate constant k^{B-II} was noticeably smaller than k^{B-I} , i.e., k^{B-II}
151 $= 2.02 \text{ s}^{-1}$ ($\tilde{\chi}^2 = 0.52$, $p > 0.94$) (Fig. 3D). Therefore, there are two types of bullet
152 complexes; one (we refer to as Type I bullet) leads to the formation of Type I football and the
153 other bullet (we refer to as Type II bullet) leads to the formation of Type II football. However,
154 the ratio of the rate constants $k^{B-I}/k^{B-II} \approx 1.36$ cannot account for the probabilities of
155 occurrence of Type I and Type II footballs (i.e., ~ 0.67 and ~ 0.33 , respectively), as described
156 below. The rate constants, $k^{F-I} = 0.49 \text{ s}^{-1}$ and $k^{B-I} = 2.75 \text{ s}^{-1}$, provide the probabilities of
157 appearance of Type I football and Type I bullet as 0.85 and 0.15, respectively, which is
158 apparently inconsistent with those mentioned above, even considering the presence of Type II
159 process. This discrepancy is due to the finite time observation of the reaction cycle (Note S2).

160 Type I football could possibly be classified into two subtypes responsible for the
161 formation of Type I and Type II bullet complexes but it is not the case. This is because the rate
162 of first-order transition from Type I football to Type II bullet was nearly identical to that from
163 Type I football to Type I bullet (Fig. S1). This conclusion was also supported by the fact that
164 both Type I and Type II bullets are formed after Type II football, with respective probabilities
165 similar to those of occurrence of Type I and Type II bullets after Type I football (probabilities:

166 449/671 \approx 0.67 for Type I bullet formation and 222/671 \approx 0.33 for Type II bullet formation).
167 In fact, the numbers of events that Type II process occurred in the n -th round in succession
168 were 67 ($N_2 = 172$), 19 ($N_3 = 53$) and 4 ($N_4 = 15$), where N_n ($n = 2-4$) represents the total
169 number of Type I and Type II bullet complexes formed after Type II football in the n -th round.
170 Thus, the probability of going through Type II process is approximately kept constant at \sim 0.33,
171 irrespective of the number of successive rounds of Type II process. As such, the two types of
172 bullet complexes always occur with respective constant probabilities, after either type of
173 football complex.

174

175 **Kinetic reaction scheme**

176 From above results as well as analyses described below, the reaction scheme for
177 GroEL–GroES interaction in the steady-state ATPase cycle was constructed (Fig. 4). The
178 reaction cycle proceeds through two distinct main and side pathways, where Type-I and
179 Type-II footballs are formed, respectively. Branching into the two pathways occurs at and is
180 determined by the bullet complexes. The main pathway is consistent with a symmetric
181 chaperonin cycle as proposed previously [24]. By contrast, in the side pathway the product
182 formed by decay of Type-II football is the same as the previous bullet regarding the
183 *cis/trans*-ring arrangement. That is, the GroES that has been bound since before and when the
184 reaction reaches the branching point never dissociates while the complex is going through the
185 side pathway. Therefore, its residence time, \sim 7.5 s (or longer when the complex proceeds in
186 succession to the side pathway), is significantly longer than that in the main pathway, \sim 4.4 s.
187 On contrary, the resident time of the second bound GroES (\sim 2.6 s) in the side pathway, which
188 is identical to the lifetime of Type-II football, is significantly shorter than the residence time
189 of the early bound GroES ($>$ \sim 7.5 s) as well as the residence time of bound GroES in the main
190 cycle (\sim 4.4 s).

191 From the values obtained above for k^{F-I} , k^{B-I} , k^{F-II_1} , k^{F-II_2} and k^{B-II} and from the probability
192 of occurrence of Type II bullet, $r \approx 1/3$, we obtained the average cycle time of GroEL–GroES
193 interaction, $\langle T_c \rangle \approx 6.33$ s, in a way described in Note S3. Supposing that 14 ATP molecules
194 are hydrolysed per GroEL molecule during $\langle T_c \rangle$, the steady-state ATPase activity is estimated
195 to be 2.2 s^{-1} per GroEL molecule. This estimated value is somewhat larger than but similar to
196 the value of 1.5 s^{-1} per GroEL molecule measured biochemically for GroEL–GroES in the
197 presence of an unfoldable substrate protein, α -lactalbumin [38], the same substrate protein as
198 that used in the present study.

199 Type II football in the side pathway shown in pale colors (Fig. 4) indicates an intermediate
200 state that is apparently the same as but different from Type II football initially formed upon
201 GroES binding. Existence of this intermediate state was deduced from the histogram of
202 lifetime for Type II football as mentioned above (Fig. 3B). Regarding Type I football shown
203 in pale colors (Fig. 4), we discuss in the next section.

204

205 **Kinetics undergone by bound GroES in the main pathway**

206 Previous single-molecule fluorescence microscopy measurements have shown that
207 dissociation of GroES from a GroEL ring occurs in two steps, through formation of one
208 kinetic intermediate [36,39]. In these studies, however, measurements were performed under
209 the condition that only one GroES was bound to GroEL (i.e, at a low concentration of GroES,
210 4 nM). Here, we examined the kinetics undergone by a bound GroES in the main circular
211 pathway under the condition that the football complexes were predominantly formed in the
212 presence of 1 μ M GroES. Figure 3E shows a histogram for the residence time of GroES. As
213 was the case with the previous studies, the distribution of the resident time showed a
214 maximum but significantly deviated from the curve best fitted to a sequential two-step
215 reaction ($\tilde{\chi}^2 = 1.51$, $p = 0.016$; Fig. 3E, green lines). For details of the residence time
216 analysis, see Notes S4 and S5. It would be most plausible that before final dissociation the
217 bound GroES simply undergoes the first football complex, the following bullet complex and
218 the second football complex in this order. However, the histogram largely deviates from the
219 corresponding curve (Fig. S2). A deviation was also noticed, although in a less extent, even
220 when the histogram was fitted to a sequential three-step reaction without restriction ($\tilde{\chi}^2 =$
221 0.92 , $p = 0.60$), as depicted in the cumulated number of GroES dissociation events (Fig. 3E,
222 blue lines). In this fitting (Fig. 3E, right, blue line), a significant advance is evident at the
223 initial phase in the lag period, compared to the experimental data (Fig. 3E, right, black dots).
224 Therefore, we postulate that the bound GroES undergoes three intermediates (besides the
225 initial football complex) before its dissociation. The histogram was well fitted to a curve for a
226 sequential four-step reaction with rate constants of $k_1 = 0.92 \text{ s}^{-1}$, $k_2 = 0.90 \text{ s}^{-1}$, $k_3 = 2.81 \text{ s}^{-1}$,
227 and $k_4 = 0.51 \text{ s}^{-1}$ ($\tilde{\chi}^2 = 0.70$, $p = 0.90$) (Fig. 3E, solid red lines). The cycle time of the main
228 pathway calculated from the values of these four rate constants and $k^{\text{B-I}}$ becomes 4.89 s, very
229 close to that calculated from the values of $k^{\text{B-I}}$ and $k^{\text{F-I}}$, i.e., $2 \times (1/k^{\text{F-I}} + 1/k^{\text{B-I}}) \sim 4.80 \text{ s}$.

230 However, precisely determining four rate constants from one histogram is difficult. In
231 addition, the histogram does not tell the order of reactions corresponding to these four rate

232 constants. Therefore, we constructed a sequential four-step reaction model by considering
233 several issues, as well as reassessing the histogram under plausible restrictions, as described
234 below. First, the values of $k_3 = 2.81 \text{ s}^{-1}$ and $k_4 = 0.51 \text{ s}^{-1}$ are similar to the values of $k^{B-I} = 2.75$
235 s^{-1} and $k^{F-I} = 0.49 \text{ s}^{-1}$, respectively, indicating that the reaction step corresponding to k_3 occurs
236 at decay of the bullet complex, while the reaction step corresponding to k_4 occurs at decay of
237 either the initial or final football. Moreover, the sum of the values of $1/k_1$ and $1/k_2$, $\sim 2.2 \text{ s}$,
238 approximately coincides with $1/k^{F-I}$ ($\sim 2.04 \text{ s}$). It is well known that substrate protein is
239 encapsulated into the internal cavity of GroEL after the binding of ATP and GroES to the
240 *trans*-ring, which instantly induces movement of the apical domain of the newly formed
241 *cis*-ring. This apical domain movement has been reported to occur in $0.56\text{--}1.47 \text{ s}$ (rate
242 constant, $0.68\text{--}1.8 \text{ s}^{-1}$) after ATP addition, depending on particular substrate protein [40].
243 Since the values of k_1 and k_2 are in this range, either k_1 or k_2 is very likely to represent the rate
244 of encapsulation. Therefore, two successive reaction steps corresponding to k_1 and k_2 occur
245 during the decay of the initial football complex (see Fig. 4). Therefore, the rate constant k_4 can
246 now be assigned to the rate of final dissociation of the second bound GroES (at the decay of
247 the last football complex). However, the dissociation of another (i.e., early bound) GroES
248 from the initial football occurs in one step, suggesting that this GroES dissociation occurs in
249 parallel to the encapsulation reaction as well as the following unspecified reaction
250 (corresponding to either k_1 or k_2) occurring in the opposite ring. Because of $1/k_1 + 1/k_2 \approx 1/$
251 k^{F-I} , completion of this unspecified reaction must be synchronized with the dissociation of the
252 early bound GroES. Therefore, the encapsulation reaction as well as the apical domain
253 movement does not seem to affect the counter ring. Collectively, we conclude that after
254 GroES binds to a GroEL ring this GroES undergoes the football complex (depicted in pale
255 colors in Figure 4), the following bullet complex and the last football complex, in this order.
256 Following this scheme, we reassessed the histogram for the residence time of GroES under
257 the restriction of $1/k_1 + 1/k_2 = 1/k^{F-I}$, $k_3 = k^{B-I}$ and $k_4 = k^{F-I}$, resulting in $k_1 = 1.14 \text{ s}^{-1}$ and $k_2 =$
258 0.87 s^{-1} ($\tilde{\chi}^2 = 0.73$, $p = 0.88$). The fitting curve obtained by this reassessment (Fig. 3E,
259 dashed red lines) was nearly indistinguishable from the initial one (Fig. 3E, solid red lines).
260 Note that $k_1 = 1.14 \text{ s}^{-1}$ is identical to the value of k^{F-II}_1 .

261

262 Discussion

263 The acquired HS-AFM images of GroEL–GroES interaction in the presence of
264 α -lactalbumin indisputably displayed that the football complexes are indeed primarily formed

265 during the repeated reaction cycles. Moreover, the HS-AFM images showed that in the main
266 pathway the two rings of GroEL operate alternately, as previously postulated [21,24,25].
267 Cooperative interactions between the two rings must govern this rhythmic, alternate operation.
268 In a prevailing view [2,4], a negative cooperative effect between the two rings has been
269 considered to inhibit ATP binding to the *trans*-ring until one ATP turnover is completed in the
270 *cis*-ring, resulting in exclusive formation of the bullet complexes in the reaction cycle. Our
271 results are inconsistent with this view. However, this prevailing view has now been somewhat
272 modified by a recent fluorescence cross-correlation spectroscopy study [38]. This study
273 showed that symmetric complexes are formed by 54% (close to our observation, 67%) and
274 23% in the presence of unfoldable substrate proteins α -lactalbumin and α -casein, respectively,
275 whereas in the presence of foldable substrate proteins they are formed by less than 10% [38].
276 In the near future, this dependence on substrate proteins should be further assessed using
277 different methods including HS-AFM, because formation of football complexes with
278 populations much larger than 10% has been reported even in the presence of foldable
279 substrate proteins [17–23,26,27]. In another model, although for the case of absence of
280 substrate protein, ADP dissociation from the *trans*-ring has been considered to limit the
281 reaction cycle, resulting in the accumulation of bullet complexes. In fact, when ATP and ADP
282 coexist in solution, ADP has been shown to be bound to the *trans*-ring [20,41]. Moreover, it
283 has been shown that even after the detachment of GroES from the *cis*-ring ADP resides in the
284 same ring [42,43]. However, in a related model, this negative cooperativity effect on the ADP
285 release from the *trans*-ring has been considered to be weakened by substrate protein bound to
286 the same ring. Therefore, binding of ATP and GroES to the *trans*-ring is accelerated [24,41],
287 and hence, the football complex is considered to be formed during the chaperonin cycle
288 [22,25].

289 However, as shown in our HS-AFM observation, Type I bullet stays for $1/k^{B-I} \sim 0.36$ s
290 even in the presence of substrate protein and 1 μ M GroES. This lifetime is much longer than
291 the time required for GroES binding to the ATP-bound *trans*-ring, considering the
292 second-order rate constant for GroES binding in the presence of substrate protein, $1-3 \times 10^7$
293 $M^{-1}s^{-1}$ [40] and the GroES concentration used here. As such, regarding ADP dissociation,
294 negative cooperativity still effectively acts on the *trans*-ring even in the presence of substrate
295 protein. This suppression of ADP release in the asymmetric bullet complex is reminiscent of
296 handover-hand movement of myosin V on actin; its identical two heads alternately take the
297 leading and trailing positions. This alternate process is made possible by strain-mediated

298 suppression of ADP release from the leading head [30,44]. Therefore, suppression of ADP
299 release in an asymmetric structure seems to be a common strategy for alternate operation of
300 two-engine ATPase systems.

301 In the main pathway (see Fig. 4), after binding to the *trans*-ring of GroEL the bound
302 GroES undergoes three intermediates before dissociation (besides the initial football complex
303 itself), as revealed by its residence time analysis. Two of the three intermediates are Type I
304 bullet and the last football complex. This coincidence of the intermediate species indicates
305 that the two rings communicate with each other in these two intermediate states. As to Type I
306 bullet, a negative cooperativity effect exists, as mentioned above. In the final football
307 complex a positive cooperativity effect must also exist that induces the final dissociation of
308 the GroES. In order for this positive cooperative effect to engender, a certain reaction must
309 have proceeded in the opposite ring, until reaching or just before the final dissociation of the
310 bound GroES. During this period, encapsulation of substrate protein into the cavity occurs in
311 the new *cis*-ring but does not seem affect the opposite ring because the encapsulation occurs
312 earlier than the final dissociation of GroES and because this dissociation occurs in one step.
313 The rate of ATP hydrolysis to ADP+Pi in the presence of foldable substrate proteins has been
314 reported to be in the range of 0.31 s^{-1} – 0.36 s^{-1} [39, 45]. Taking into account the higher
315 ATPase activities of GroEL in the presence of unfoldable substrate proteins [38], the value of
316 k^{F-I} (0.49 s^{-1}) can be considered to correspond to the rate of ATP hydrolysis into ADP+Pi.
317 Therefore, it is very likely that ATP hydrolysis in the new *cis*-ring triggers Pi release and
318 hence final dissociation of GroES from the opposite ring.

319 To understand the cause of branching into the side pathway, here we summarize its major
320 properties. (i) The early bound GroES never dissociates; rather the newly bound GroES
321 dissociates at the exit of the side pathway, (ii) the formation of Type II bullet leads to the side
322 pathway, (iii) the bullet complex formed at the exit of the side pathway can proceed to either
323 pathway, (iv) the probabilities of branching into the main and side pathways ($\sim 2/3$ and $\sim 1/3$,
324 respectively) cannot be accounted for by the rate constants, $k^{B-I} = 2.75\text{ s}^{-1}$ and $k^{B-II} = 2.02\text{ s}^{-1}$,
325 (v) the rate of Type II football formation (2.02 s^{-1}) is smaller than that of Type I football
326 formation (2.75 s^{-1}), (vi) Type II football decays in two steps, whereas Type I football decays
327 in one step, (vii) Type II football has a moderately longer lifetime ($\sim 2.6\text{ s}$) than Type I football
328 ($\sim 2.04\text{ s}$), and (viii) importantly the side pathway occurs even in the absence of substrate
329 protein (Fig. 5).

330 It has been postulated that the substrate protein initially tethered to the apical domain of
331 GroEL would have two or three different fates [46,47]. However, these fates have nothing to
332 do with the pathway branching (Note S6) because the side pathway occurs even in the
333 absence of substrate protein. Although there is no direct evidence at this stage, we consider
334 that incomplete exchange of nucleotide at the *trans*-ring may cause sidetracking into the side
335 pathway, while complete exchange of seven ADPs with seven ATPs assures the GroE system
336 to go through the main pathway. In Type I bullet, the rate of ADP dissociation from the
337 *trans*-ring is suppressed, as described above. This suppression provides an enough time for
338 the substrate protein to be released from the *trans*-ring but in turn could possibly cause
339 frequent, incomplete nucleotide replacement at the *trans*-ring, which would direct the reaction
340 process towards the side pathway. This hypothesis is consistent with partial stochasticity of
341 ATP hydrolysis, as suggested by a previous study [25], as well as with all observed properties
342 of Type II process. For example, the partially remained ADP should somewhat reduce the
343 affinity of the *trans*-ring for GroES, consistent with the smaller rate constant $k^{B-II} = 2.02 \text{ s}^{-1}$
344 than $k^{B-I} = 2.75 \text{ s}^{-1}$. This weaker GroEL–GroES association would possibly reduce the rate of
345 ATP hydrolysis to ADP–Pi in the new *cis*-ring, consistent with the longer lifetime of Type II
346 football than Type I football. Moreover, the hydrolysis of reduced number of ATP molecules
347 in the new *cis*-ring must significantly reduce its positive cooperative effect on the dissociation
348 of the early bound GroES from the opposite ring, consistent with the fact that in the side
349 pathway the early bound GroES never dissociates.

350

351 **Materials and methods**

352

353 **Proteins**

354 The D490C GroEL was produced by site-directed mutagenesis. D490C GroEL and
355 wild-type GroES were expressed in *Escherichia coli* XL1-Blue and purified as described
356 previously [48]. Purified D490C GroEL was labeled with biotin by the reaction with
357 biotin-PEAC₅-maleimide for 30 min at 25°C as described [35]. The molar ratio of biotin
358 introduced per GroEL subunit was determined to be 0.8 using
359 4'-hydroxyazobenzene-2-carboxylic acid (Wako Chemicals, Osaka) [49]. Streptavidin and
360 α -lactalbumin were purchased (Wako Chemicals, Osaka and Nacalai Tesque, Kyoto,
361 respectively).

362

363 **Streptavidin 2D crystals**

364 Streptavidin 2D crystals were prepared on the surface of mica-supported lipid planar
365 bilayer containing biotin-lipid, as described [35]. Briefly, the mica-supported lipid bilayer was
366 first obtained by a vesicle fusion method. After washing the excess lipids, crystallization of
367 streptavidin was performed by deposition of streptavidin (0.2 mg/ml) dissolved in
368 crystallization buffer (10 mM HEPES, 150 mM NaCl and 2 mM CaCl₂, pH 7.4) on the lipid
369 bilayer surface, followed by incubation for 2 h. Then, the streptavidin 2D crystals were
370 chemically stabilized by the application of 10 mM glutaraldehyde mixed with the
371 crystallization buffer. After 5 min incubation, the reaction was quenched using 20 mM Tris
372 added to the crystallization buffer.

373

374 **High-speed atomic force microscopy**

375 Observations were carried out in amplitude modulation mode using a laboratory-built
376 HS-AFM setup [28,29]. Small cantilevers used are custom made by Olympus (spring constant
377 of 0.1 N/m and the first resonant frequency of 0.8 MHz in water). Sharp tips were fabricated
378 on the original tip by electron beam deposition and then by argon-plasma etching. The
379 biotinylated D490C GroEL diluted to 25 nM was applied to the streptavidin 2D crystals. After
380 3 min incubation, unattached GroEL was washed out with buffer. HS-AFM imaging was
381 performed at an imaging rate of ~4 fps, at 22 °C in a solution containing 25 mM HEPES-KOH,
382 100 mM KCl and 5 mM MgCl₂, 1 μM GroES, 1 μM bovine α-lactalbumin, 2 mM ATP and 2
383 mM DTT. For HS-AFM imaging in the absence of substrate protein shown in Fig. 5, bovine
384 α-lactalbumin was omitted from the solution.

385

386 **Data Analyses**

387 The species of GroEL–GroES complexes were able to be identified by visual inspection
388 of HS-AFM images, thanks to the high resolution images. The analyses of lifetimes of the
389 bullet and football complexes as well as the residence time of bound GroES were performed
390 with a software program constructed using Mathematica 10.2 (Wolfram Research, Illinois).
391 The histograms of lifetime for Type I football and Type I and Type II bullets were fitted to
392 single-exponential decay functions. The histogram of lifetime for Type II football was fitted to
393 an equation for a sequential two-step reaction (Note S1). The residence time of GroES in the
394 main pathway was fitted to equations of sequential two-step, three-step or four-step reactions
395 (Note S4). The fitting results were also depicted with curves obtained by using corresponding

396 equations for the cumulated number of events that occur during the period from time Δt to
397 time $n\Delta t$, where n is integer and Δt is the frame time of imaging (Note S4). This depiction
398 provides better inspection for the fitting results than the use of curves for lifetime or residence
399 time distribution. The details of data analysis for sequential three and four-step reactions are
400 described in Note S5.

401

402 **References**

403

- 404 [1] F.U. Hartl, A. Bracher, M. Hayer-Hartl, Molecular chaperones in protein folding and
405 proteostasis, *Nature* 475 (2011) 324–332.
- 406 [2] F.U. Hartl, M. Hayer-Hartl, Molecular chaperones in the cytosol: from nascent chain
407 to folded protein, *Science* 295 (2002) 1852–1858.
- 408 [3] K. Braig, Z. Otwinowski, R. Hegde, D.C. Boisvert, A. Joachimiak, A.L. Horwich, et
409 al., The crystal structure of the bacterial chaperonin GroEL at 2.8 Å, *Nature* 371
410 (1994) 578–586.
- 411 [4] A.L. Horwich, W.A. Fenton, Chaperonin-mediated protein folding: using a central
412 cavity to kinetically assist polypeptide chain folding, *Q. Rev. Biophys.* 42 (2009)
413 83–116.
- 414 [5] T.K. Chaudhuri, V.K. Verma, A. Maheshwari, GroEL assisted folding of large
415 polypeptide substrates in *Escherichia coli*: present scenario and assignments for the
416 future, *Prog. Biophys. Mol. Biol.* 99 (2009) 42–50.
- 417 [6] A.I. Jewett, J.E. Shea, Reconciling theories of chaperonin accelerated folding with
418 experimental evidence, *Cell. Mol. Life Sci.* 67 (2010) 255–276.
- 419 [7] D.K. Clare, P.J. Bakkes, H. van Heerikhuizen, S.M. van der Vies, H.R. Saibil,
420 Chaperonin complex with a newly folded protein encapsulated in the folding chamber,
421 *Nature* 457 (2009) 107–110.
- 422 [8] J.S. Weissman, C.M. Hohl, O. Kovalenko, Y. Kashi, S. Chen, K. Braig, et al.,
423 Mechanism of GroEL action: productive release of polypeptide from a sequestered
424 position under GroES, *Cell* 83 (1995) 577–587.
- 425 [9] M. Mayhew, A.C. da Silva, J. Martin, H. Erdjument-Bromage, P. Tempst, F.U. Hartl,
426 Protein folding in the central cavity of the GroEL-GroES chaperonin complex, *Nature*
427 379 (1996) 420–426.
- 428 [10] O. Yifrach, A. Horovitz, Nested cooperativity in the ATPase activity of the oligomeric
429 chaperonin GroEL, *Biochemistry* 34 (1995) 5303–5308.
- 430 [11] S.G. Burston, N.A. Ranson, A.R. Clarke, The origins and consequences of asymmetry
431 in the chaperonin reaction cycle, *J Mol Biol* 249 (1995) 138–152.

- 432 [12] A. Horovitz, K.R. Willison, Allosteric regulation of chaperonins, *Curr Opin Struct*
433 *Biol* 15 (2005) 646–651.
- 434 [13] Z. Xu, A.L. Horwich, P.B. Sigler, The crystal structure of the asymmetric
435 GroEL-GroES-(ADP)₇ chaperonin complex, *Nature* 388 (1997) 741–750.
- 436 [14] H.S. Rye, S.G. Burston, W.A. Fenton, J.M. Beechem, Z. Xu, P.B. Sigler, et al., Distinct
437 actions of *cis* and *trans* ATP within the double ring of the chaperonin GroEL, *Nature*
438 388 (1997) 792–798.
- 439 [15] H.S. Rye, A.M. Roseman, S. Chen, K. Furtak, W.A. Fenton, H.R. Saibil, et al.,
440 GroEL-GroES cycling: ATP and nonnative polypeptide direct alternation of
441 folding-active rings, *Cell* 97 (1999) 325–338.
- 442 [16] M. Schmidt, K. Rutkat, R. Rachel, G. Pfeifer, R. Jaenicke, P. Viitanen, et al.,
443 Symmetric complexes of GroE chaperonins as part of the functional cycle, *Science*
444 265 (1994) 656–659.
- 445 [17] A. Azem, M. Kessel, P. Goloubinoff, Characterization of a functional
446 GroEL₁₄(GroES₇)₂ chaperonin hetero-oligomer, *Science* 265 (1994) 653–656.
- 447 [18] H. Sparrer, K. Rutkat, J. Buchner, Catalysis of protein folding by symmetric
448 chaperone complexes, *Proc Natl Acad Sci USA* 94 (1997) 1096–1100.
- 449 [19] A. Koike-Takeshita, M. Yoshida, H. Taguchi, Revisiting the GroEL-GroES reaction
450 cycle via the symmetric intermediate implied by novel aspects of the GroEL(D398A)
451 mutant, *J Biol Chem* 283 (2008) 23774–23781.
- 452 [20] T. Sameshima, T. Ueno, R. Iizuka, N. Ishii, N. Terada, K. Okabe, et al., Football- and
453 bullet-shaped GroEL-GroES complexes coexist during the reaction cycle, *J Biol Chem*
454 283 (2008) 23765–23773.
- 455 [21] T. Sameshima, R. Iizuka, T. Ueno, J. Wada, M. Aoki, N. Shimamoto, et al.,
456 Single-molecule study on the decay process of the football-shaped GroEL-GroES
457 complex using zero-mode waveguides, *J Biol Chem* 285 (2010) 23159–23164.
- 458 [22] T. Sameshima, R. Iizuka, T. Ueno, T. Funatsu, Denatured proteins facilitate the
459 formation of the football-shaped GroEL-(GroES)₂ complex, *Biochem J* 427 (2010)
460 247–254.
- 461 [23] Takei, Y., Iizuka, R., Ueno, T. & Funatsu, T. Single-molecule observation of protein
462 folding in symmetric GroEL-(GroES)₂ complexes. *J. Biol. Chem.* **287**, 41118–41125
463 (2012).
- 464 [24] X. Ye, G.H. Lorimer, Substrate protein switches GroE chaperonins from asymmetric to
465 symmetric cycling by catalyzing nucleotide exchange, *Proc Natl Acad Sci USA* 110
466 (2013) E4289–E4297.
- 467 [25] D. Yang, X. Ye, G.H. Lorimer, Symmetric GroEL:GroES₂ complexes are the
468 protein-folding functional form of the chaperonin nanomachine, *Proc Natl Acad Sci*
469 *USA* 110 (2013) E4298–E4305.

- 470 [26] X. Fei, X. Ye, N.A. LaRonde, G.H. Lorimer, Formation and structures of
471 GroEL:GroES₂ chaperonin footballs, the protein-folding functional form, Proc Natl
472 Acad Sci USA 111 (2014) 12775–12780.
- 473 [27] A. Koike-Takeshita, T. Arakawa, H. Taguchi, T. Shimamura, Crystal structure of a
474 symmetric football-shaped GroEL:GroES₂-ATP₁₄ complex determined at 3.8Å reveals
475 rearrangement between two GroEL rings, J. Mol. Biol. 426 (2014) 3634–3641.
- 476 [28] T. Ando, N. Kodera, E. Takai, D. Maruyama, K. Saito, A. Toda, A high-speed atomic
477 force microscope for studying biological macromolecules, Proc Natl Acad Sci USA 98
478 (2001) 12468–12472.
- 479 [29] T. Ando, T. Uchihashi, T. Fukuma, High-speed atomic force microscopy for
480 nano-visualization of dynamic biomolecular processes, Prog Surf Sci 83 (2008)
481 337–437.
- 482 [30] N. Kodera, D. Yamamoto, R. Ishikawa, T. Ando, Video imaging of walking myosin V
483 by high-speed atomic force microscopy, Nature 468 (2010) 72–76.
- 484 [31] T. Uchihashi, R. Iino, T. Ando, H. Noji, High-speed atomic force microscopy reveals
485 rotary catalysis of rotorless F₁-ATPase, Science 333 (2011) 755–758.
- 486 [32] T. Ando, T. Uchihashi, S. Scheuring, Filming biomolecular processes by high-Speed
487 atomic force microscopy, Chem Rev 114 (2014) 3120–3188.
- 488 [33] M.B. Viani, L.I. Pietrasanta, J.B. Thompson, A. Chand, I.C. Gebeshuber, J.H. Kindt, et
489 al., Probing protein-protein interactions in real time, Nat Struct Biol 7 (2000)
490 644–647.
- 491 [34] M. Yokokawa, C. Wada, T. Ando, N. Sakai, A. Yagi, S.H. Yoshimura, et al.,
492 Fast-scanning atomic force microscopy reveals the ATP/ADP-dependent
493 conformational changes of GroEL, EMBO J 25 (2006) 4567–4576.
- 494 [35] D. Yamamoto, N. Nagura, S. Omote, M. Taniguchi, T. Ando, Streptavidin 2D crystal
495 substrates for visualizing biomolecular processes by atomic force microscopy,
496 Biophys. J. 97 (2009) 2358–2367.
- 497 [36] H. Taguchi, T. Ueno, H. Tadakuma, M. Yoshida, T. Funatsu, Single-molecule
498 observation of protein-protein interactions in the chaperonin system, Nat Biotechnol
499 19 (2001) 861–865.
- 500 [37] M. Beißinger, K. Rutkat, J. Buchner, Catalysis, commitment and encapsulation during
501 GroE-mediated folding, J Mol Biol 289 (1999) 1075–1092.
- 502 [38] S. Haldar, A.J. Gupta, X. Yan, G. Miličić, F.U. Hartl, M. Hayer-Hartl,
503 Chaperonin-assisted protein folding: Relative population of asymmetric and
504 symmetric GroEL:GroES complexes, J Mol Biol 427 (2015) 2244–2255.
- 505 [39] T. Ueno, H. Taguchi, H. Tadakuma, M. Yoshida, T. Funatsu, GroEL mediates protein
506 folding with a two successive timer mechanism, Mol Cell 14 (2004) 423–434.
- 507 [40] F. Motojima, C. Chaudhry, W.A. Fenton, G.W. Farr, A.L. Horwich, Substrate

- 508 polypeptide presents a load on the apical domains of the chaperonin GroEL, Proc Natl
509 Acad Sci USA 101 (2004) 15005–15012.
- 510 [41] J.P. Grason, J.S. Gresham, G.H. Lorimer, Setting the chaperonin timer: a two-stroke,
511 two-speed, protein machine, Proc Natl Acad Sci USA 105 (2008) 17339–17344.
- 512 [42] J.P. Grason, J.S. Gresham, L. Widjaja, S.C. Wehri, G.H. Lorimer, Setting the
513 chaperonin timer: the effects of K^+ and substrate protein on ATP hydrolysis, Proc Natl
514 Acad Sci USA 105 (2008) 17334–17338.
- 515 [43] D. Madan, Z. Lin, H.S. Rye, Triggering protein folding within the GroEL-GroES
516 complex, J Biol Chem 283 (2008) 32003–32013.
- 517 [44] T.J. Purcell, H.L. Sweeney, J.A. Spudich, A force-dependent state controls the
518 coordination of processive myosin V, Proc Natl Acad Sci USA 102 (2005)
519 13873–13878.
- 520 [45] M. Suzuki, T. Ueno, R. Iizuka, T. Miura, T. Zako, R. Akahori, et al., Effect of the
521 C-terminal truncation on the functional cycle of chaperonin GroEL: Implication that
522 the C-terminal region facilitates the transition from the folding-arrested to the
523 folding-competent state, J Biol Chem 283 (2008) 23931–23939.
- 524 [46] F. Motojima, M. Yoshida, Polypeptide in the chaperonin cage partly protrudes out and
525 then folds inside or escapes outside, EMBO J 29 (2010) 4008–4019.
- 526 [47] M. J. Todd, G.H. Lorimer, D. Thirumalai, Chaperonin-facilitated protein folding:
527 optimization of rate and yield by an iterative annealing mechanism, Proc Natl Acad
528 Sci USA 93 (1996) 4030–4035.
- 529 [48] M. Taniguchi, T. Yoshimi, K. Hongo, T. Mizobata, Y. Kawata, Stopped-flow
530 fluorescence analysis of the conformational changes in the GroEL apical domain, J
531 Biol Chem 279 (2004) 16368–16376.
- 532 [49] Y. Kunioka, T. Ando, Innocuous labeling of the subfragment-2 region of skeletal
533 muscle heavy meromyosin with a fluorescent polyacrylamide nanobead and
534 visualization of individual heavy meromyosin molecules, J Biochem 119 (1996)
535 1024–1032.

536
537

538 **Acknowledgements**

539

540 We thank Prof. Masasuke Yoshida for critical reading of the draft and for valuable
541 comments and Dr. Masaaki Taniguchi for technical assistance. This work was supported by
542 grants to T.A.: KAKENHI, Grant-in-Aids for Basic Research S (#20221006 and #24227005)
543 and Research on Innovative Area (Research in a proposed research area; #26119003) from

544 Japan Society for the Promotion of Science, and CREST program of Japan Science and
545 Technology Agency.

546

547 **Appendix A. Supplementary Data**

548 Supplementary data to this article can be found online at <http://>

549

550

551 **Figure legends**

552

553 **Fig. 1. GroEL-GroES interaction observed by HS-AFM.** (A) Schematic illustration of the
554 assay system used for HS-AFM imaging of GroEL–GroES interaction. Streptavidin was
555 two-dimensionally crystallized on a mica-supported lipid bilayer surface containing
556 biotin-lipid. D490C GroEL biotinylated at 490C locating at its equatorial domain was
557 immobilized on the streptavidin 2D crystal surface through the biotin-streptavidin linkage.
558 The bulk solution includes 1 μ M GroES, 1 μ M denatured (disulfide-reduced) lactalbumin and
559 2 mM ATP. (B) HS-AFM images captured at \sim 4 fps of GroES binding to and dissociating
560 from the GroEL rings. The dashed lines indicate the positions of toroid ends of the GroEL
561 molecule. The arrowheads indicate GroES bound to GroEL. Z-scale: 15 nm. (C) Time course
562 of the association and dissociation of GroES at each ring of GroEL observed in (B).

563

564 **Fig. 2. Population of GroEL–GroES complexes and their dynamic appearance and**
565 **disappearance observed by HS-AFM.** (A) Population of species in the presence of 2 mM
566 ATP and 1 μ M substrate protein (disulfide-reduced lactalbumin). “n” indicates the total
567 number of frames captured. (B) Patterns and relative proportion of the sequential GroES
568 binding and release events observed during the steady-state ATPase cycle. “n” indicates the
569 total number of events detected.

570

571 **Fig. 3. Histograms and their best fitting results for lifetime of GroEL–GroES complexes**
572 **and residence time of bound GroES.** The insets in A–E show the cumulated numbers of
573 corresponding events (gray bars) together with curves calculated using rate constants obtained
574 by fitting of their histograms to corresponding models (blue lines for A–D; blue, green and
575 red lines for E). “n” attached to each inset indicates the total number of observed events. (A)
576 Histogram (gray bars) for lifetime of Type I football and the best result of its fitting to a single

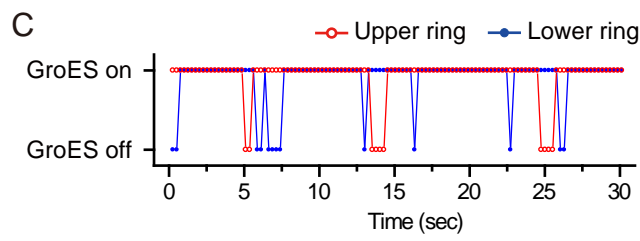
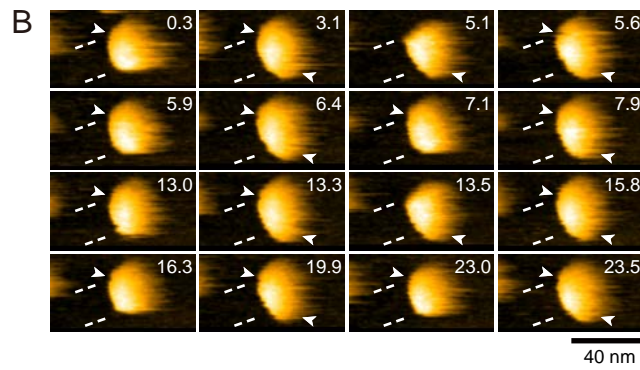
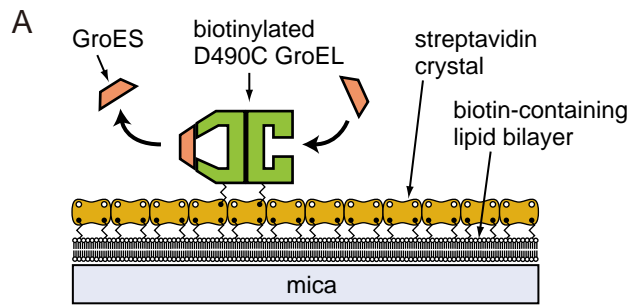
577 exponential function (blue line). (B) Histogram (gray bars) for lifetime of Type II football and
578 the best result of its fitting to a sequential two-step reaction model (blue line). (C) Histogram
579 (gray bars) for lifetime of Type I bullet and the best result of its fitting to a single exponential
580 function (blue line). (D) Histogram (gray bars) for lifetime of Type II bullet and the best result
581 of its fitting to a single exponential function (blue line). (E) Histogram (gray bars) for
582 residence time of GroES and the best result of its fitting to a sequential four-step reaction
583 model (solid and dashed red lines). The dashed red lines show the best result of fitting
584 performed under the restriction of $k_3 = k^{B-1}$ and $k_4 = k^{F-1}$, while the solid red lines show the
585 best result of fitting performed without restriction. The green and blues lines show the best
586 results obtained when the histogram for residence time of GroES was fitted to sequential
587 two-step and three-step reaction models, respectively. The inset (right) shows the initial
588 lag-time phase of the cumulated number of GroES dissociation events.

589

590 **Fig. 4. Kinetic reaction scheme of GroEL–GroES interaction revealed by HS-AFM**
591 **imaging.** The football complexes shown in pale colors are apparently the same as but
592 kinetically different from the respective football complexes initially formed upon GroES
593 binding. The solid black arrows indicate reactions in the main circular pathway, whereas the
594 solid green arrows indicate those in the side pathway. The dashed red arrows indicate reaction
595 processes estimated from the residence time of bound GroES. The order of k^{F-II}_1 and k^{F-II}_2
596 was assigned as shown here, considering the fact that the value of $k^{F-II}_2 = 0.59 \text{ s}^{-1}$ is smaller
597 than the smallest value reported for the rate of substrate encapsulation reaction that occurs
598 after GroES binding to the same ring of GroEL. The order of k_1 and k_2 was assigned as shown
599 here, considering the fact that the value of k_1 is identical to the value of k^{F-II}_1 . In the side
600 pathway, the coexistence of ATP and ADP in one ring is shown but hypothetical.

601

602 **Fig. 5. Successive HS-AFM images showing dynamic GroEL–GroES interaction in the**
603 **absence of substrate protein.** The numbers shown are the frame number. As indicated at
604 frame 102, the polarity of the bullet complex is unchanged from the previous bullet (frame
605 89) after a round of dissociation and association of GroES. Although not shown in this figure,
606 7 out of total 47 GroES binding and release events observed showed formation of Type II
607 football. The imaging was performed 22 °C in a solution containing 25 mM HEPES-KOH,
608 100 mM KCl and 5 mM MgCl₂, 1 μM GroES, 2 mM ATP and 2 mM DTT. Imaging rate, ~4
609 fps; imaging area, 95 × 41 nm².



A complex ratio (%)



0.4

GroEL



32.8

bullet

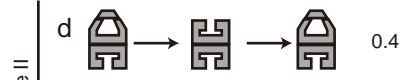
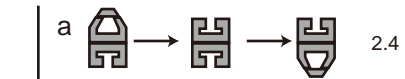


66.8

football

n = 12714

B GroES binding-release action ratio (%)



n = 1012

